JOURNAL OF SPACECRAFT AND ROCKETS
Vol. 35, No. 6, November–December 1998

Aerodynamic Interference for Hypersonic Missiles at Low Angle of Attack

H. F. Nelson* and Derek G. Hillstrom†
University of Missouri–Rolla, Rolla, Missouri 65409-0050

An Euler code is used to predict the flowfield over a hypersonic missile and to determine the carryover factors $K_{W(B)}$, fin lift in the presence of the body, and $K_{B(W)}$, lift produced by the body in the presence of the fins. The missile is assumed to have cruciform, delta fins in the + orientation and an aspect ratio of 1.529. Results are presented as a function of fin span at Mach 6, 8, and 10, for a 2-deg angle of attack. Two ratios of specific heats, 1.4 and 1.3, are considered to partially account for vibrational excitation effects. Both carryover factors have approximately the same variation with fin size as their slender body predictions. The values of $K_{W(B)}$ and $K_{B(W)}$ are 2 for a missile without fins. The value of $K_{W(B)}$ decreases toward 1 and $K_{B(W)}$ decreases toward 0.20 as the fin span becomes large. At a fixed fin size, $K_{W(B)}$ decreases and $K_{B(W)}$ increases as Mach number increases. At a fixed value of fin size and Mach number, both $K_{W(B)}$ and $K_{B(W)}$ increase slightly due to vibrational excitation effects.

Nomenclature

A_F = wing-planform area formed by two fins joined at their root chord, m^2
AR = aspect ratio of wing formed by joining two fins at their root chord
C_N = normal force coefficient referenced to A_F
C_{N_C} = normal force coefficient of entire missile
C_{N_F} = normal force coefficient of fin alone
$C_{N_{F,\alpha}}$ = normal force curve slope, fin alone
$C_{N_{\mathrm{FB}}}$ = forebody-alone normal force coefficient
$C_{N_{\mathrm{FB},\alpha}}$ = normal force curve slope, forebody alone
$K_{B(W)}$ = body–fin interference factor
$K_{W(B)}$ = fin–body interference factor
$L_{B(W)}$ = body lift in presence of fin, N
L_C = entire missile configuration lift, N
L_F = fin-alone lift, N
L_{FB} = forebody-alone lift, N
$L_{W(B)}$ = fin lift in presence of body, N
M = freestream Mach number
P = local pressure/(freestream pressure)
q = freestream dynamic pressure, N/m^2
R = body radius at end of nose cone (1, any units)
R_{LE} = body radius at root chord leading edge = 1.436 R, units of R
S = fin span measured from body centerline, units of R
Z = missile axial distance measured from nose, units of R
α = angle of attack of body–fin combination, 2 deg
α_{eq} = equivalent angle of attack, deg
α_F = angle of attack of fin alone, 2 deg
γ = ratio of specific heats
ϵ = fin semivertex angle, 20 deg
θ = body flare angle, 1 deg
Λ = fin leading-edge sweep angle, 70 deg
ϕ = angular position, deg (0 at top)

Introduction

THERE is interest in developing hypersonic missiles that fly in the Mach 8–12 range to destroy enemy ballistic missiles within the first 100 s after launch.[1] The goal is to intercept and to destroy the ballistic missiles such that the debris falls near the launch facility.

Design of high-speed missiles is facilitated by accurate and fast computational techniques to predict the flowfield around the missile. Conceptual and preliminary design of missiles requires rapid analytical and empirical methods to do tradeoff studies to optimize the missile configuration for both performance and stability and control. As design goals become more challenging, the inclusion of all of the necessary factors, i.e., Mach number, angle of attack, fin shape, and chemistry effects, becomes crucial in the tradeoff studies.

Missiles have been designed using slender body theory (SBT) and linear potential theory (LPT), which has led to the development of the equivalent-angle-of-attack method.[2–5] Missiles have also been designed using semiempirical methods that are based on an extensive database, which is the basis of the Aeroprediction Code AP95.[6,7]

The objective of this paper is to use the ZEUS code[8] to predict the hypersonic flowfield and to evaluate the hypersonic fin–body and body–fin carryover factors $K_{W(B)}$ and $K_{B(W)}$ as functions of fin size, Mach number, and γ. Numerical codes allow one to investigate a wide range of configurations and flight parameters and provide detailed flowfield properties not attainable with empirical techniques. The results of this research project can be used to improve the database for Missile DATCOM and AP95.

Background

Component-Buildup Methods

Component-buildup methods are fast and economical ways of evaluating fundamental preliminary design parameters such as force and moment coefficients and stability derivatives. A specific component-buildup method is the equivalent-angle-of-attack method. This method considers forces on individual missile components separately and then adds the individual forces to find the total missile normal force coefficient. Interference factors are used to account for the mutual interference between the missile components. From Fig. 1 the lift on the entire missile configuration is

$$L_C = L_{B(W)} + L_{W(B)} = L_{\mathrm{FB}} + \left[L_{B(W)} - L_{\mathrm{FB}}\right] + L_{W(B)} \tag{1}$$

This can be rewritten as

$$L_C = L_{\mathrm{FB}} + \left[\frac{L_{W(B)}}{L_F} + \frac{L_{B(W)} - L_{\mathrm{FB}}}{L_F}\right] L_F \tag{2}$$

Equation (2) can be written in terms of the carryover factors as

$$L_C = L_{\mathrm{FB}} + \left[K_{W(B)} + K_{B(W)}\right] L_F \tag{3}$$

Note that the lift on the missile configuration consists of the lift on the forebody alone, L_{FB}, and the lift on the fin alone, L_F, modified

Presented as Paper 98-0680 at the AIAA 36th Aerospace Sciences Meeting and Exhibit, Reno, NV, Jan. 12–15, 1998; received Jan. 26, 1998; revision received July 13, 1998; accepted for publication July 13, 1998. Copyright © 1998 by the American Institute of Aeronautics and Astronautics, Inc. All rights reserved.

*Professor of Aerospace Engineering, Thermal Radiative Transfer Group, Department of Mechanical and Aerospace Engineering and Engineering Mechanics. Associate Fellow AIAA.
†Student, Department of Mechanical and Aerospace Engineering and Engineering Mechanics. Student Member AIAA.

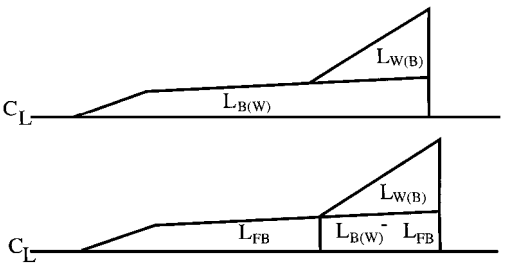

Fig. 1 Lift components on missile configuration.

by the two interference factors, $K_{W(B)}$ and $K_{B(W)}$. Accurate functional equations for $K_{W(B)}$ and $K_{B(W)}$ decrease computation time in conceptual and preliminary design. The values of L_{FB} and L_F are usually readily available. SBT defines the body-alone lift as $L_{FB} = 2\pi q \alpha R^2$. LPT defines L_F for a delta fin with supersonic leading edges as $L_F = 4\alpha_F q A_F / \sqrt{(M^2 - 1)}$.

The equivalent angle of attack, is defined by dividing Eq. (3) by qA_F to get

$$C_{N_C} = C_{N_{FB}} + \left[K_{W(B)} + K_{B(W)}\right] C_{N_F} \tag{4}$$

At small angles of attack, C_N is linear with angle of attack, so that $C_N = \alpha C_{N,\alpha}$ and Eq. (4) becomes

$$C_{N_C} = C_{N_{FB,\alpha}} \alpha + \left[K_{W(B)} + K_{B(W)}\right] C_{N_{F,\alpha}} \alpha_F \tag{5}$$

Now the equivalent angle of attack α_{eq} is defined as

$$\alpha_{eq} = \left[K_{W(B)} + K_{B(W)}\right] \alpha_F \tag{6}$$

when sideslip and vorticity effects are neglected. Thus, the normal force on the missile fin–body configuration is

$$C_{N_C} = C_{N_{FB,\alpha}} \alpha + C_{N_{F,\alpha}} \alpha_{eq} \tag{7}$$

If sideslip effects, vorticity effects, fin deflection effects, multiple sets of fins, and large angle of attack are considered, Eq. (7) becomes more complicated.[3]

Missile Data

Experimental data used in missile design consist of fin-alone, body-alone, and entire-missile wind-tunnel measurements. Stallings and Lamb[9] carried out a systematic investigation of fin-alone experiments to determine C_{N_F} using surface pressure measurements. The pressure distributions were integrated to obtain C_{N_F} for Mach numbers from 1.60 to 4.60 and angles of attack up to 60 deg. The fins had aspect ratios of 0.5, 1.0, and 2.0 and taper ratios of 0, 0.5, and 1.

Results of a wind-tunnel test program have been reported by Burns and Bruns.[10] The program involved testing fin–body models from Mach 0.6 to 3.95 at angles of attack from −2 to 30 deg. Twelve different fins were used with aspect ratios between 1 and 6 and taper ratios of 0 and 0.5. A third data set is available,[‡] but it is not completely reduced and correlated.

Nielsen[11] analyzed some of the data in the NASA Tri-Service database to extract the values of $K_{W(B)}$ and $K_{B(W)}$ at Mach numbers between 2.5 and 4.5 as a function of angle of attack from 0 to 40 deg. He found that at small angles of attack $K_{W(B)}$ did not deviate very much from SBT and at high angles of attack $K_{W(B)}$ tended to go toward 1. The carryover $K_{B(W)}$ tended to have significant deviations from SBT.

Because of boundary-layer effects on hypersonic missiles, a Navier–Stokes numerical analysis is desirable. Bhutta and Lewis[12] used the three-dimensional parabolized Navier–Stokes equations to predict the flowfields around supersonic and hypersonic missiles. They considered angles of attack of 0, 2, and 5 deg and investigated the effects of fin thickness and fin deflection.

[‡]B. Shaw and W. Sawyer, NASA Langley Research Center Tri-Service Missile Data Base, transmitted by J. M. Allen to University of Missouri–Rolla, 1992 (formal documentation in process).

Numerical predictions of $K_{W(B)}$ and $K_{B(W)}$ have been done at the University of Missouri–Rolla using Euler codes at supersonic velocities for various missile configurations.[13–20] Euler equations significantly reduce the computer run time without degrading the quality of the results at supersonic speeds.

Analysis

The fin–body carryover due to upwash, $K_{W(B)}$, is defined as the lift produced by the fin in the presence of the body divided by the lift produced by the fin alone:

$$K_{W(B)} = \frac{L_{W(B)}}{L_F} \tag{8}$$

When $K_{W(B)} \geq 1$, positive interference occurs, and the fin in the fin–body combination produces more lift than the fin alone.

The body–fin interference parameter $K_{B(W)}$ is defined as the difference between the lift produced by the body in the presence of the fin and the lift produced by the forebody divided by the lift produced by the fin alone:

$$K_{B(W)} = \frac{\left[L_{B(W)} - L_{FB}\right]}{L_F} \tag{9}$$

When $K_{B(W)} \geq 0$, the body in the presence of the fin produces more lift than the body alone.

Fin-Alone Lift L_F

The terms $K_{W(B)}$ and $K_{B(W)}$ are normalized by L_F. The value of L_F is computed by determining the lift produced by an infinitely thin wing composed of two fins joined at their root chords. Linearized potential theory was used to determine L_F. For a fin alone with supersonic leading edges, L_F is

$$L_F = \frac{4\alpha_F q A_F}{\sqrt{(M^2 - 1)}} \tag{10}$$

Equation (10) was used to determine L_F for all of the cases considered herein. Fins with subsonic edges were not considered.

Slender Body Theory

SBT yields simple equations for $K_{W(B)}$ and $K_{B(W)}$ as a function of S/R only. Nielsen[21] developed a theoretical equation for $K_{W(B)}$ using SBT:

$$K_{W(B)} = \frac{1}{\pi(\delta - 1)^2} \times \left[\frac{\pi}{2}\left(\frac{\delta^2 - 1}{\delta}\right)^2 + \frac{\delta^2 - 1}{\delta} \arcsin\frac{\delta^2 - 1}{\delta^2 + 1} - \frac{2(\delta^2 - 1)}{\delta}\right] \tag{11}$$

where $\delta = S/R$. Nielsen's SBT equation for $K_{B(W)}$ is

$$K_{B(W)} = [(\delta + 1)/\delta]^2 - K_{W(B)} \tag{12}$$

Equations (11) and (12) are derived for a cylinder-shaped body with planar delta fins.

SBT assumes that the flowfield is irrotational and isentropic and that axial-flow derivatives are negligible compared with crossflow derivatives. These assumptions limit SBT to small angles of attack. Vortices, shock waves, and expansion waves are not considered. The Euler equations allow for shock and expansion waves and account for vorticity and rotational effects[8]; therefore, they allow the computational modeling of the interference factors to be a function of M, γ, and α in addition to S/R.

Methodology

ZEUS is a finite volume Euler code that was developed by the U.S. Naval Weapons Center to solve the three-dimensional Euler equations.[8,22] It employs a second-order Godunov method that marches axially along the missile using a multiple-zone grid in the cross-sectional plane. ZEUS computational time was reduced by utilizing pitch plane symmetry and a uniform 36 × 36 ($r \times \phi$) grid with two zones. Flowfield solutions were obtained between

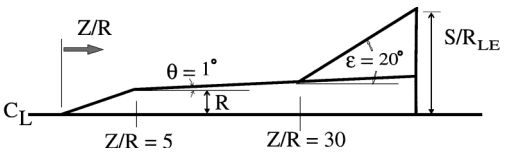

Fig. 2 Missile configuration.

the body and the bow shock. To improve the accuracy over the fins, the Courant–Friedrichs–Lewy number, which controls the computational marching step, was reduced from 0.9 to 0.6. CPU times on the University of Missouri–Rolla Hewlett Packard Series 700 computer workstation ranged from 10 to 15 min.

The accuracy of the numerical calculations was verified by comparing current results with those of the example case from Ref. 22. Several different gridding sizes were used, with the result that a 36 × 36 grid was optimum with regard to computer time and accuracy. The accuracy of the ZEUS code is well documented.[17,18,20,22–24] Experimental data have recently been obtained that can be used to further evaluate the accuracy of the ZEUS code.[10]

Missile Geometry

The missile used in this research is shown in Fig. 2. It had a conical nose with a length-to-radius ratio of 5 and a cylindrical body with a 1-deg flare. The fins were infinitely thin flat plates with triangular planforms and $\Lambda = 70$ deg. For delta fins joined at their root chord to form a planar wing, the aspect ratio is

$$AR = \frac{4\tan^2\epsilon}{\tan\epsilon - \tan\theta} \tag{13}$$

Missile configurations with both planar fin and + cruciform fin orientations were considered. The fin leading edge was located at $Z/R = 30$, and so the fins were not influenced by the cone–cylinder junction. Because ZEUS is an axial marching code, one run includes a spectrum of S/R ratios. In other words, at each Z/R value greater than 30, each axial step yields a new solution for a missile with larger fins. The term $R_{\rm LE}$ is the body radius at $Z/R = 30$. [Recall that $R = 1$ in any units; thus, $R_{\rm LE}/R = 1 + 25\tan(\theta) = 1.436$.] The term $S/R_{\rm LE}$ is used as the independent variable for $K_{W(B)}$ and $K_{B(W)}$ interference factor calculations. The term $L_{\rm FB}$ is the lift produced by the forebody for Z/R between 0 and 30, $L_{B(W)}$ is the lift produced by the body in the presence of the fin for Z/R greater than 30, and $L_{W(B)}$ is the lift produced by the fin in the presence of the body. The Appendix presents some calculation details.

Flight Conditions

The purpose of this research is to extend the database for $K_{W(B)}$ and $K_{B(W)}$ into the hypersonic Mach number range. The $K_{W(B)}$ and $K_{B(W)}$ data are developed for Mach numbers of 6, 8, and 10 at $\gamma = 1.3$ and 1.4. The angle of attack was 2 deg. The fin aspect ratio was 1.529. A γ of 1.3 was used to account for vibrational excitation effects in hypersonic flow. The $K_{W(B)}$ and $K_{B(W)}$ values over the fins are plotted vs $S/R_{\rm LE}$, and the data over the whole body are plotted vs Z/R.

Results and Discussion

Pressure is not influenced greatly by attached boundary layers; consequently, the ZEUS solutions give accurate forces and moments due to pressure at low angles of attack. Base drag and skin friction are not considered in this analysis. Figures 3 and 4 show pressure (ratioed to the freestream value) contours at three axial positions along the body for Mach 8 at $\gamma = 1.4$ and 1.3, respectively.

The $Z/R \approx 30$ cross sections show roughly constant pressure at a value near 1 because the fin is so small that it does not influence the pressure field. Figures 3 and 4 clearly show the position of the fin leading-edge shock and expansion waves for $Z/R \approx 38$ and 48. The nondimensional pressure is about 1.7 below the fin and about 0.5 above the fin. Near the fin root chord the shock is farther below the fin than it is near the fin tip because the shock near the root chord is generated at the root chord leading edge that is located far upstream from the crossflow plane, whereas the shock near the tip is generated close to the given crossflow plane. Thus, the oblique shock located near the root chord has ample distance to move away from the fin planform. The same physical effect occurs with the expansion wave above the fin. The pressure for $\gamma = 1.4$ is slightly higher below the fin than it is for $\gamma = 1.3$; however, changing γ from 1.4 to 1.3 does not change the pressure significantly.

Streamlines for crossflow velocity are shown in Fig. 5 for $M = 8$ and $\gamma = 1.4$ at $Z/R = 47.8$ and in Fig. 6 for $M = 8$ and $\gamma = 1.3$ at $Z/R = 47.7$. The streamlines follow the shock underneath the fin and show the formation of a vortex above the fin. The crossflow is subsonic everywhere.

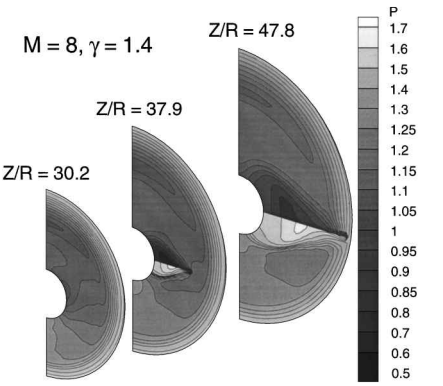

Fig. 3 Contours of pressure divided by the freestream pressure at Z/R = 30.2, 37.9, and 47.8 for M = 8 and γ = 1.4.

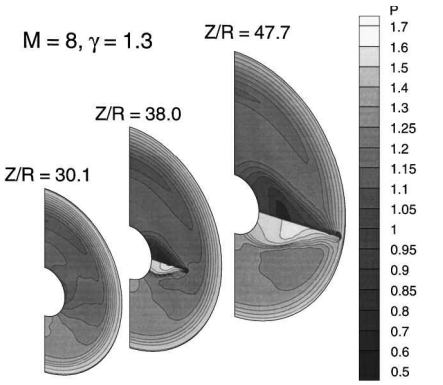

Fig. 4 Contours of pressure divided by the freestream pressure at Z/R = 30.1, 38, and 47.7 for M = 8 and γ = 1.3.

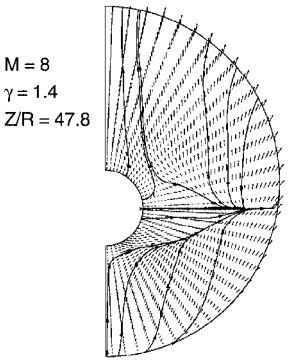

Fig. 5 Streamlines for crossflow velocity for M = 8 and γ = 1.4.

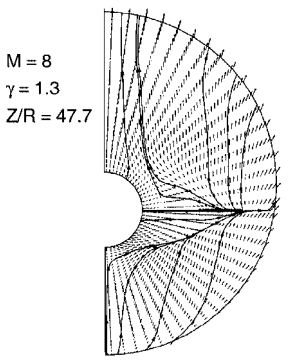

Fig. 6 Streamlines for crossflow velocity for M = 8 and γ = 1.3.

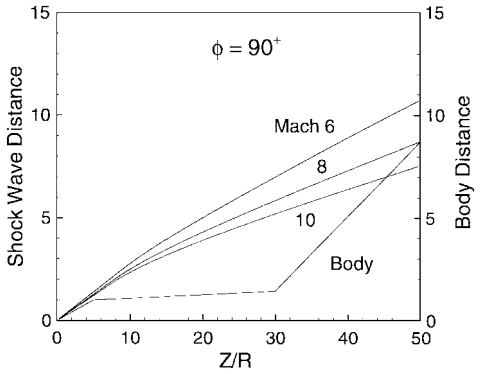

Fig. 7 Bow shock radius along body at M = 6, 8, and 10 and γ = 1.4.

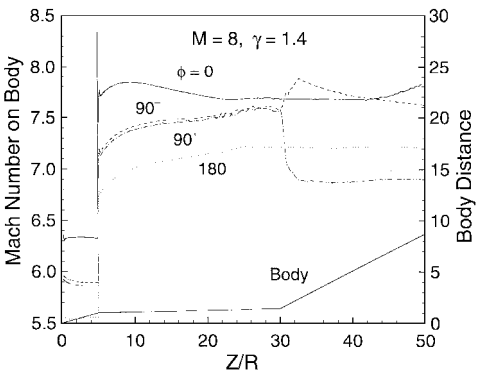

Fig. 8 Mach number on the body for M = 8 and γ = 1.4.

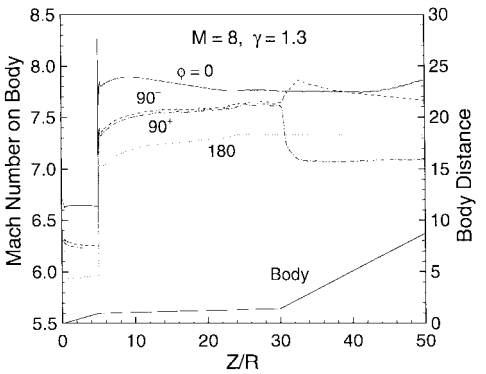

Fig. 9 Mach number on the body for M = 8 and γ = 1.3.

Figure 7 shows the bow shock position at $\phi = 90$ deg as a function of Mach number and Z/R. It also shows the missile shape (body distance on right-hand ordinate) in nondimensional units as a function of Z/R. The angle $\phi = 90$ deg is in the plane of the horizontal fin, which is used to calculate the fin forces. The bow shock location at a specific value of Z/R moves closer to the body as M increases. At Mach 8 the bow shock touches the horizontal fin at $Z/R = 50$, whereas at Mach 10 the bow shock intersects the horizontal fin at $Z/R \simeq 45$. The flowfield is calculated between the body and the bow shock; consequently, the Mach 10 solution for $Z/R \geq \approx 45$ ignores the effects of the fin area outside the bow shock. This effect limits the maximum value of S/R_{LE} to 5. The top and bottom fins of the cruciform + configuration are infinitely thin and are located on a plane of symmetry, and so the solutions for the horizontal fin are independent of these fins penetrating the bow shock.

Figures 8 and 9 show Mach number on the body as a function of Z/R at four angular positions—$\phi = 0, 90^-, 90^+$, and 180 deg (top of body, top of fin, bottom of fin, and bottom of body)—for a freestream Mach number of 8 at $\gamma = 1.4$ and 1.3, respectively. The body shape is plotted along the bottom as a function of Z/R with the radial distance on the right axis. The Mach number on the nose cone is less than 8 due to passage through the bow shock. The sharp increase in Mach number at $Z/R = 5$ is caused by the expansion waves at the nose cone, flared-cylinder junction. The Mach number

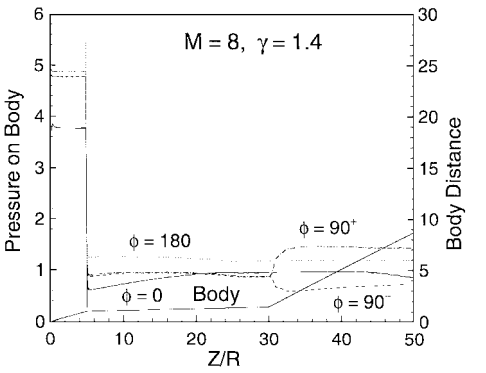

Fig. 10 Pressure divided by the freestream pressure on the body for M = 8 and γ = 1.4.

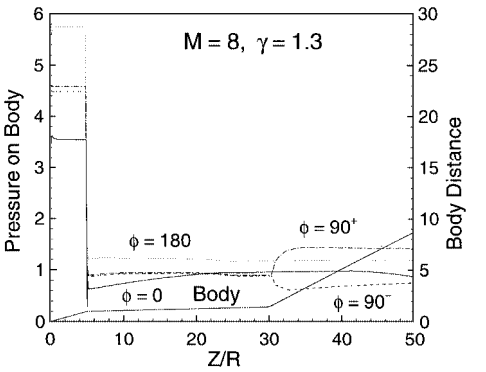

Fig. 11 Pressure divided by the freestream pressure on the body for M = 8 and γ = 1.3.

then relaxes to a steady value until it encounters the fins. At the horizontal fin, the flow at $\phi = 90^-$ (above fin) expands due to the 2-deg angle of attack, and the Mach number increases and then relaxes as Z/R increases further. The Mach number at $\phi = 90^+$ (below fin) decreases behind the shock wave at $Z/R = 30$ and then relaxes to about 7 as Z/R increases. The Mach number along the body at $\phi = 0$ and 180 (top and bottom of body) remains relatively steady at approximately 7.8 and 7.4, respectively.

Figures 10 and 11 show the pressure (ratioed to the freestream value) as a function of Z/R on the body at four angular positions: $\phi = 0, 90^-, 90^+$, and 180 deg (top of body, top of fin, bottom of fin, and bottom of body). The data are for Mach 8 at $\gamma = 1.4$ and 1.3, respectively. The body shape is plotted along the bottom as a function of Z/R with the radial distance on the right axis.

The pressure on the nose cone is greater than the freestream pressure due to the jump across the bow shock. The sharp decrease in pressure at $Z/R = 5$ is caused by the expansion waves at the nose cone flared-cylinder junction. The pressure then relaxes to a steady value near 1 until it encounters the fins. At the horizontal fins, the flow at $\phi = 90^-$ (above fins) expands due to the 2-deg angle of attack, and the pressure decreases and then relaxes back toward 1 as Z/R increases further. The pressure at $\phi = 90^+$ (below fins) increases due to the fin leading-edge shock and then relaxes slightly as Z/R increases. The pressure along the body at $\phi = 0$ (top) and 180 (bottom) remains relatively steady with increasing Z/R at approximately 1 and 1.1, respectively.

Carryover, $K_{W(B)}$

Figure 12 presents $K_{W(B)}$ as a function of S/R_{LE} at $M = 6, 8$, and 10 for $\gamma = 1.4$ and 1.3. At a given Mach number $K_{W(B)}$ decreases toward 1 as the fins become larger. Interference effects between the fin and the body are negligible when $K_{W(B)} = 1$. Figure 12 shows that $K_{W(B)}$ decreases at a specific value of S/R_{LE} (fixed fin size) as M increases and that $K_{W(B)}$ increases slightly as γ decreases from 1.4 to 1.3. The numerical data become inaccurate at small values of S/R_{LE} due to the small number of pressure data points on the fin. Therefore, the data have been extrapolated for S/R_{LE} less than 1.5 so that they go to the theoretical limit of 2 at $S/R_{\mathrm{LE}} = 1$. The SBT

Table 1 $K_{W(B)}$ at Mach 6, 8, and 10

	$\gamma = 1.4$			$\gamma = 1.3$			
S/R	6	8	10	6	8	10	SBT
1.00	2.000	2.000	2.000	2.000	2.000	2.000	2.000
1.05	1.945	1.900	1.720	1.946	1.905	1.740	1.948
1.10	1.880	1.805	1.630	1.885	1.823	1.650	1.896
1.20	1.784	1.677	1.520	1.793	1.695	1.535	1.810
1.30	1.706	1.590	1.450	1.716	1.605	1.462	1.739
1.40	1.650	1.533	1.400	1.658	1.548	1.410	1.678
1.50	1.609	1.494	1.365	1.615	1.505	1.375	1.627
1.60	1.580	1.466	1.335	1.585	1.476	1.345	1.582
1.70	1.555	1.445	1.320	1.560	1.455	1.330	1.543
1.80	1.535	1.430	1.310	1.540	1.440	1.320	1.508
1.90	1.516	1.416	1.300	1.521	1.426	1.310	1.478
2.00	1.500	1.405	1.290	1.505	1.415	1.304	1.450
2.10	1.485	1.394	1.283	1.489	1.405	1.296	1.426
2.20	1.471	1.383	1.276	1.476	1.395	1.291	1.404
2.30	1.458	1.375	1.271	1.462	1.385	1.285	1.384
2.40	1.445	1.365	1.265	1.450	1.376	1.279	1.366
2.50	1.433	1.357	1.260	1.439	1.368	1.274	1.349
2.60	1.423	1.349	1.255	1.427	1.360	1.269	1.334
2.70	1.412	1.341	1.251	1.417	1.353	1.265	1.320
2.80	1.402	1.335	1.246	1.406	1.345	1.260	1.307
2.90	1.392	1.328	1.243	1.397	1.338	1.256	1.295
3.00	1.382	1.321	1.239	1.388	1.332	1.252	1.284
3.10	1.374	1.315	1.235	1.378	1.325	1.248	1.274
3.20	1.365	1.309	1.231	1.370	1.319	1.244	1.265
3.30	1.357	1.303	1.228	1.362	1.313	1.240	1.256
3.40	1.349	1.298	1.224	1.354	1.307	1.236	1.247
3.50	1.342	1.292	1.221	1.346	1.301	1.233	1.239
3.60	1.334	1.287	1.218	1.339	1.296	1.229	1.232
3.70	1.327	1.282	1.215	1.332	1.291	1.226	1.225
3.80	1.321	1.277	1.212	1.325	1.285	1.222	1.219
3.90	1.314	1.272	1.209	1.319	1.280	1.219	1.212
4.00	1.308	1.267	1.206	1.312	1.276	1.216	1.206
4.10	1.302	1.262	1.204	1.306	1.271	1.214	1.201
4.20	1.296	1.258	1.201	1.300	1.266	1.211	1.196
4.30	1.290	1.254	1.199	1.294	1.262	1.208	1.191
4.40	1.285	1.250	1.197	1.289	1.257	1.206	1.186
4.50	1.279	1.245	1.195	1.283	1.253	1.204	1.181
4.60	1.274	1.241	1.193	1.278	1.249	1.202	1.177
4.70	1.269	1.238	1.191	1.273	1.245	1.200	1.173
4.80	1.264	1.234	1.190	1.268	1.241	1.198	1.169
4.90	1.259	1.230	1.188	1.263	1.237	1.196	1.165
5.00	1.255	1.227	1.187	1.258	1.234	1.194	1.162

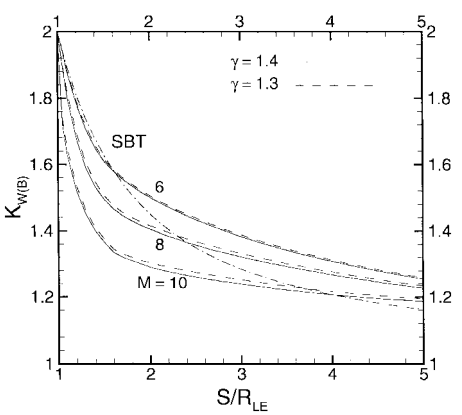

Fig. 12 $K_{W(B)}$ vs S/R_{LE} for M = 6, 8, and 10 at γ = 1.4 and 1.3.

value of $K_{W(B)}$ is also shown in Fig. 12. SBT predicts that $K_{W(B)} = 2$ when there is no fin and approaches 1 as S/R_{LE} goes to infinity. The SBT value for $K_{W(B)}$ falls off faster with S/R_{LE} than the ZEUS predictions. Recall that SBT is only a function of S/R_{LE}. Note that the SBT prediction has the same general trend as the Euler results, so that it is a useful approximation to $K_{W(B)}$ for rough calculations.

The effect of vibrational excitation on $K_{W(B)}$ is shown by changing γ from 1.4 to 1.3. Note that vibrational excitation effects are small and that they increase with Mach number as one would expect.

Table 2 $K_{B(W)}$ at Mach 6, 8, and 10

	$\gamma = 1.4$			$\gamma = 1.3$			
S/R	6	8	10	6	8	10	SBT
1.00	2.000	2.000	2.000	2.000	2.000	2.000	2.000
1.10	1.639	1.790	1.849	1.649	1.806	1.870	1.749
1.20	1.329	1.588	1.698	1.345	1.617	1.736	1.551
1.30	1.069	1.396	1.548	1.088	1.432	1.597	1.391
1.40	0.860	1.213	1.397	0.879	1.252	1.453	1.260
1.50	0.702	1.039	1.247	0.717	1.076	1.304	1.151
1.60	0.598	0.874	1.096	0.610	0.904	1.150	1.059
1.70	0.525	0.757	0.946	0.535	0.782	0.992	0.980
1.80	0.471	0.670	0.834	0.479	0.692	0.874	0.912
1.90	0.430	0.602	0.747	0.437	0.622	0.782	0.852
2.00	0.397	0.549	0.678	0.403	0.566	0.709	0.800
2.10	0.371	0.506	0.622	0.377	0.521	0.650	0.753
2.20	0.350	0.470	0.575	0.355	0.484	0.601	0.712
2.30	0.333	0.441	0.536	0.337	0.453	0.559	0.675
2.40	0.318	0.415	0.502	0.322	0.427	0.524	0.641
2.50	0.306	0.394	0.473	0.309	0.404	0.493	0.611
2.60	0.295	0.375	0.448	0.298	0.384	0.467	0.583
2.70	0.286	0.358	0.426	0.289	0.367	0.444	0.558
2.80	0.278	0.344	0.407	0.281	0.352	0.423	0.535
2.90	0.271	0.331	0.390	0.273	0.339	0.405	0.513
3.00	0.265	0.319	0.374	0.267	0.327	0.388	0.493
3.10	0.259	0.309	0.360	0.261	0.316	0.374	0.475
3.20	0.254	0.300	0.348	0.256	0.306	0.360	0.458
3.30	0.250	0.291	0.336	0.251	0.297	0.348	0.442
3.40	0.245	0.283	0.326	0.247	0.289	0.337	0.428
3.50	0.242	0.276	0.316	0.243	0.281	0.326	0.414
3.60	0.238	0.270	0.307	0.240	0.275	0.317	0.401
3.70	0.235	0.264	0.299	0.236	0.268	0.308	0.389
3.80	0.233	0.258	0.291	0.234	0.263	0.299	0.377
3.90	0.230	0.253	0.284	0.231	0.257	0.292	0.366
4.00	0.228	0.249	0.277	0.229	0.252	0.285	0.356
4.10	0.225	0.244	0.271	0.226	0.248	0.278	0.346
4.20	0.223	0.240	0.265	0.224	0.244	0.272	0.337
4.30	0.222	0.236	0.259	0.222	0.240	0.267	0.329
4.40	0.220	0.233	0.255	0.221	0.236	0.261	0.320
4.50	0.218	0.230	0.250	0.219	0.233	0.257	0.313
4.60	0.217	0.227	0.245	0.217	0.230	0.252	0.305
4.70	0.215	0.224	0.241	0.216	0.227	0.248	0.298
4.80	0.214	0.221	0.237	0.214	0.224	0.244	0.291
4.90	0.213	0.219	0.234	0.213	0.222	0.240	0.285
5.00	0.211	0.217	0.230	0.212	0.220	0.236	0.278

Table 1 gives numerical data for $K_{W(B)}$ from the ZEUS calculations for M = 6, 8, and 10 at γ = 1.4 and 1.3 as a function of S/R_{LE}. It also gives the SBT values. These data can be used in conceptual and preliminary design.

Carryover, $K_{B(W)}$

Figure 13 shows $K_{B(W)}$ as a function of S/R_{LE} at Mach 6, 8, and 10 for γ = 1.3 and 1.4. Predictions from ZEUS and the SBT result are shown. The value of $K_{B(W)}$ from SBT decreases from 2 to 0 as S/R_{LE} increases from 1 to infinity. Recall that the SBT predictions are only a function of fin geometry. They are independent of M and α. Thus, from Fig. 13 the effect of Mach number is easily seen. The value of $K_{B(W)}$ from ZEUS is inaccurate at small S/R_{LE} due to the small number of data points on the fin; therefore, the data for S/R_{LE} less than 1.5 have been extrapolated to go to the SBT theoretical limit of 2 as $S/R_{LE} = 1$.

As M increases, $K_{B(W)}$ at a given value of S/R_{LE} increases. This behavior is opposite to the trend shown by $K_{W(B)}$. As M increases, the carryover between the fin and the body moves backward along Mach lines on the body surface. Some of the interference occurs behind the body. This implies that the $K_{B(W)}$ will become important on the afterbody. In the present study the effects of afterbodies were not investigated. Reference 20 considers these effects.

The effect of chemistry on $K_{B(W)}$ is shown by changing γ from 1.4 to 1.3. Note that chemistry effects are small and that they increase with Mach number.

Table 2 presents numerical values of $K_{B(W)}$ from ZEUS for M = 6, 8, and 10 at γ = 1.4 and 1.3 as a function of S/R_{LE}. It also gives the SBT values. These values can be used in conceptual and preliminary design.

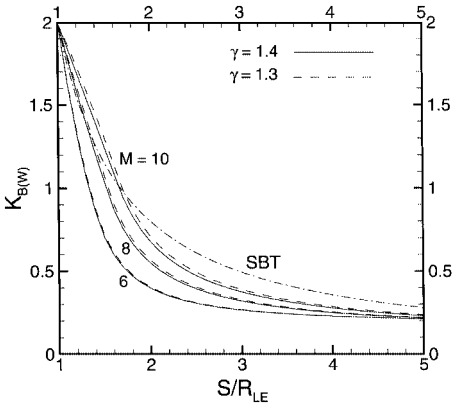

Fig. 13 $K_{B(W)}$ **vs** S/R_{LE} **for** $M = 6, 8$, **and 10 at** $\gamma = 1.4$ **and 1.3.**

Conclusions

The carryover factors $K_{W(B)}$ and $K_{B(W)}$ have been determined for Mach numbers of 6, 8, and 10 at $\gamma = 1.4$ and 1.3. Reducing γ from 1.4 to 1.3 partially accounts for the air vibrational excitation effects that occur in hypersonic flow. The angle of attack was 2 deg, and the AR was 1.529. The interference factors vary with fin size (S/R_{LE}) in a manner similar to that of SBT predictions. However, $K_{W(B)}$ and $K_{B(W)}$ also vary with Mach number and γ. The terms $K_{W(B)}$ and $K_{B(W)}$ were determined for S/R_{LE} from 1 to 5 for a missile with no afterbody. The values for $K_{W(B)}$ at $S/R_{LE} = 1$ approach the SBT theoretical value of 2. As M increases from 6 to 10, $K_{W(B)}$ at a specific fin size, S/R_{LE}, decreases and $K_{B(W)}$ increases. As S/R_{LE} approaches 5, $K_{W(B)}$ decreases to about 1.2 for all of the M values. The term $K_{B(W)}$ approaches about 0.2 as S/R_{LE} approaches 5 for all Mach numbers. Both $K_{W(B)}$ and $K_{B(W)}$ show trends similar to SBT predictions as a function of fin size.

The effect of vibrational excitation has been investigated by changing γ from 1.4 to 1.3. This effect is small; however, it increases with Mach number as one would expect.

Appendix: Postprocessor Calculations

The data generated by the ZEUS code were postprocessed to determine the $K_{W(B)}$ and $K_{B(W)}$. The normal force C_N is calculated by ZEUS for specific values of M, α, and γ. The general equation for the normal force in ZEUS is

$$F = C_N q A_{\text{ref}} \tag{A1}$$

where A_{ref} is the reference area.

The total lift on the fin in the presence of the body is defined as the sum of the forces on the top and bottom surface of the fin:

$$L_{W(B)} = F_{F(\text{top})} + F_{F(\text{bottom})} \tag{A2}$$

The total lift on the fin alone is given by linearized potential theory as

$$L_F = \frac{4\alpha}{\sqrt{M^2 - 1}} q A_F \tag{A3}$$

The term $K_{W(B)}$ can then be calculated using $L_{W(B)}$ and L_F in Eq. (8).

The calculation of $K_{B(W)}$ requires the lift produced by the forebody and the lift produced by the body in the presence of the fins. The lift on the forebody is obtained by running ZEUS from $Z/R = 0$ to the root chord leading edge, yielding

$$L_{\text{FB}} = F_{B(\text{top})} + F_{B(\text{bottom})} \tag{A4}$$

Continuing the computer run to values of Z/R beyond the root chord leading edge provides the lift on the body in the presence of the fins as

$$L_{B(W)} = \left[F_{B(\text{top})} + F_{B(\text{bottom})}\right] - L_{\text{FB}} \tag{A5}$$

Note that the lift $L_{B(W)}$ is zero at the leading edge of the fin root chord. The values for $L_{B(W)}$, L_{FB}, and L_F are then used in Eq. (9) to determine $K_{B(W)}$.

Acknowledgment

This research has been partially supported by the NASA Missouri Space Grant Consortium.

References

[1] Fulghum, D. A., "Missile Builders Compete for BPI," *Aviation Week and Space Technology*, July 1994, pp. 52, 53.

[2] Pitts, W. C., Nielsen, J. N., and Kaattri, G. E., "Lift and Center of Pressure of Wing–Body–Tail Combinations at Subsonic, Transonic, and Supersonic Speeds," NACA Rept. 1307, 1957.

[3] Hemsch, M. J., "Component Build-Up Method for Engineering Analysis of Missiles at Low-to-High Angles of Attack," *Tactical Missile Aerodynamics: Prediction Methodology*, edited by M. R. Mendenhall, Vol. 142, Progress in Astronautics and Aeronautics, AIAA, Washington, DC, 1992, pp. 115–169.

[4] Hemsch, M. J., and Nielsen, J. N., "Extension of Equivalent Angle-of-Attack Method for Nonlinear Flowfields," *Journal of Spacecraft and Rockets*, Vol. 22, No. 3, 1985, pp. 304–308.

[5] Burns, K. A., Deters, K. J., Stoy, S. L., Vukelich, S. R., and Blake, W. B., "Missile Datcom, User's Manual—Revision 6/93," Wright Lab., WL-TR-93-3043, Wright–Patterson AFB, OH, June 1993.

[6] Moore, F. G., McInville, R. M., and Hymer, T., "The 1995 Version of the NSWC Aeroprediction Code: Part I—Summary of New Theoretical Methodology," U.S. Naval Surface Warfare Center, Dahlgren Div., NSWCDD/TR-94/379, Dahlgren, VA, Feb. 1995.

[7] Moore, F. G., McInville, R. M., and Hymer, T., "The 1995 Version of the NSWCDD Aeroprediction Code: Part II—Computer Program User's Guide and Listing," U.S. Naval Surface Warfare Center, Dahlgren Div., NSWCDD/TR-95/5, Dahlgren, VA, March 1995.

[8] Wardlaw, A. B., and Davis, S. F., "A Second Order Godunov Method for Tactical Missiles," U.S. Naval Weapons Center, NSWC TR 86-506, White Oak, MD, Dec. 1986.

[9] Stallings, R. L., Jr., and Lamb, M., "Wing-Alone Aerodynamic Characteristics for High Angles of Attack at Supersonic Speeds," NASA TP-1889, July 1981.

[10] Burns, K. A., and Bruns, K. D., "Development of an Improved Carryover Interference Method for Missile Datcom," AIAA Paper 96-3395, July 1996.

[11] Nielsen, J. N., "Supersonic Wing-Body Interference at High Angles of Attack with Emphasis on Low Aspect Ratios," AIAA Paper 86-0568, Jan. 1986.

[12] Bhutta, B. A., and Lewis, C. H., "Supersonic/Hypersonic Flowfield Predictions over Typical Finned Missile Configurations," *Journal of Spacecraft and Rockets*, Vol. 30, No. 6, 1993, pp. 674–681.

[13] Jenn, A. A., and Nelson, H. F., "Sideslip Effects on Fin-Fin Interference in Supersonic Missile Aerodynamics," *Journal of Spacecraft and Rockets*, Vol. 25, No. 6, 1988, pp. 385–392.

[14] Jenn, A. A., and Nelson, H. F., "Wing Vertical Position Effects on Lift for Supersonic Delta Wing Missiles," *Journal of Spacecraft and Rockets*, Vol. 26, No. 4, 1989, pp. 210–216.

[15] Nelson, H. F., "Wing-Body Interference Lift for Supersonic Missiles with Elliptical Cross-Section Fuselages," *Journal of Spacecraft and Rockets*, Vol. 26, No. 5, 1989, pp. 322–329.

[16] Nelson, H. F., and Talpallikar, M. V., "Fin-Planform Effects on Lift and Center of Pressure for Supersonic Missiles," *Journal of Spacecraft and Rockets*, Vol. 30, No. 6, 1993, pp. 707–714.

[17] Est, B. E., and Nelson, H. F., "Wing Vertical Position Effects on Wing-Body Carryover for Noncircular Missiles," *Journal of Spacecraft and Rockets*, Vol. 31, No. 6, 1994, pp. 999–1006.

[18] Nelson, H. F., and Bossi, B. W., "Aerodynamic Interference for Supersonic Low-Aspect-Ratio Missiles," *Journal of Spacecraft and Rockets*, Vol. 32, No. 2, 1995, pp. 270–278.

[19] Est, B. E., and Nelson, H. F., "Wing-Body Carryover for Noncircular Missiles," *Journal of Spacecraft and Rockets*, Vol. 32, No. 3, 1995, pp. 426–432.

[20] Nelson, H. F., and Bossi, B. W., "Predictions of Low Aspect Ratio Missile Aerodynamics," *Journal of Spacecraft and Rockets*, Vol. 32, No. 4, 1995, pp. 596–600.

[21] Nielsen, J. N., *Missile Aerodynamics*, McGraw–Hill, New York, 1960; republished by Nielsen Engineering and Research, Mountain View, CA, 1988, Chap. 5.

[22] Wardlaw, A. B., and Priolo, F. J., "Applying the ZEUS Code," U.S. Naval Weapons Center, NSWC TR-86-508, Dahlgren, VA, Dec. 1986.

[23] Evans, J., and Wardlaw, A. B., "Prediction of Tubular Projectile Aerodynamics Using the ZEUS Euler Solver," AIAA Paper 89-0334, Jan. 1989.

[24] Priolo, F. J., and Wardlaw, A. B., "Euler Space-Marching Computations with Crossflow Separation for Missile-Type Bodies," AIAA Paper 90-0616, Jan. 1990.

R. M. Cummings
Associate Editor